Ethiopian Journal of Science and Sustainable Development

e-ISSN 2663-3205 *Volume 6 (2), 2019*

Journal Home Page: www.ejssd.astu.edu.et

Research Paper

Synthesis of Silica Supported Iron Oxide Nanoparticles for Hexavalent Chromium Removal from Aqueous Solutions

Jibril Edris, Neeraj K. Gupta, Enyew A. Zereffa*

School of Applied Natural Science, Department of Applied Chemistry Adama Science and Technology University, P.O Box 1888, Adama, Ethiopia

**Corresponding author, e-mail: enyewama@yahoo.com*

Abstract

Iron oxide nanoparticles (NPs) were synthesized by the chemical precipitation method using 1:2 ferric chloride hexahydrate ($FeCl_3.6H_2O$) and ferrous sulphate heptahydrate ($FeSO_4.7H_2O$) precursors and ammonium hydroxide (NH_4OH) precipitating agent. These NPs were evaluated for their performance as adsorbents for hexavalent chromium ions (Cr (VI)) in aqueous solutions. Silicon dioxide gel (SiO_2) was also incorporated during synthesis to improve the adsorption characteristics of the NPs. The NPs (with out and with SiO_2 gel (iron oxide NPs-SiO_2) were characterized by XRD and FTIR spectroscopy. By XRD, it was evidenced that the iron oxide NPs and iron oxide NPs-SiO_2 adsorbents were mixed oxides of magnetite (Fe_3O_4) and maghemite (γ-Fe_2O_3) with small crystallite size of 13.5 nm and 12.8 nm respectively. The mixed oxides were formed as a result of the synthesis parameters and drying temperature at 150^0C in air. The change of the black color of the just synthesized NPs to orange brown also inferred the transformation of Fe_3O_4 to γ-Fe_2O_3. Further evidence of mixed oxides is provided by the FTIR analysis wherein the characteristic bands of γ-Fe_2O_3 around 582 cm^{-1} and the distinct high-frequency shoulder in the proximity of 635 cm^{-1} to 642 cm^{-1} are evidenced besides those of Fe_3O_4.The effect of different parameters such as pH, Cr (VI) ions concentration, adsorbent dose and contact time on the efficiency of adsorption showed that the iron oxide NPs-SiO_2 adsorbent showed better performance for the removal of Cr (VI) ions under acidic pH at room temperature compared to the iron oxide NPs adsorbent. The maximum uptake of Cr (VI) ions by the iron oxide NPs-SiO_2 adsorbent increased from 80% to 96.5% by decreasing its initial concentration from 60 mg l^{-1} to 20 mg l^{-1} at optimum conditions. Analysis of the adsorption isotherms of the iron oxide NPs-SiO_2 adsorbent by the Langmuir and Freundlich models showed that the experimental data fitted well to the Langmuir model suggesting monolayer coverage of Cr (VI) ions mainly on the outer surface of the adsorbent.

Keywords: - *Iron oxide nanoparticles, Silica gel, Magnetite, Maghemite, Adsorption.*

1. Introduction

Heavy metals are among the various life-threatening pollutants present in soil and aquatic bodies and endangering the health of humans (Duruibe et al., 2007), animals (Boyd, 2010) and plants (Cheng, 2003). The global heavy metal concentration in various environments is increasing due to an increase in their use and the number of industries. Most of the industrial wastewaters contain heavy metals such as cadmium (Cd), lead (Pb), zinc (Zn), arsenic (As), cobalt (Co) and chromium (Cr) (Duruibe et al., 2007), etc.

Among these heavy metals, Cr mainly contaminates the water bodies through effluents from industrial activities such as electroplating, leather tanning, dying, mining and nuclear power plants (Smith and Ghiassi, 2006). Cr (VI) is known to cause cancer and targets the respiratory system; kidneys, liver, skin, eyes and different regulatory authorities have developed

regulations and guidelines for Cr to protect the public from potential adverse health effects. The Occupational Safety and Health Administration (OSHA) has established an 8-hour time-weighted average (TWA) exposure limit of 5 mg of Cr (VI) per cubic meter of air (5 g m^{-3}) (US Department of Labor, 2009); the National Institute for Occupational Safety and Health (NIOSH) has recommended a 10-hour time-weighted average (TWA) exposure limit for all Cr (VI) compounds of 1 µgm^{-3} Cr (VI) (NIOSH 2013); the U.S. Environmental Protection Agency (EPA) limits the maximum contaminant level of total Cr in wastewater at 0.05mg l^{-3} (Acar and Malkoc, 2004); and the World Health Organization (WHO) guideline regulates total chromium containing Cr (III), Cr (VI) and other species of chromium to be discharged below 2 mg l^{-1} (WHO, 2004).

A number of treatment methods for the removal of heavy metal ions from aqueous solutions have been reported such as reduction, ion exchange, solvent extraction, reverse osmosis, chemical precipitation, adsorption, biosorption and electrodialysis (Odeh et al., 2015). Most of these methods have certain disadvantages such as the production of large volumes of sludge, high cost of chemicals, increased concentration of dissolved solids in the effluent, high startup costs and low efficiency (Samarghandi et al., 2015).

Adsorption, however, is recognized as an effective and economical process for a wide variety of applications, especially for the removal of heavy metals from wastewaters, the exception being one of the most widely used adsorbents, i.e., activated carbon, which is expensive and possibly non-cost effective in the treatment of large wastewater volumes (Nadeem et al., 2006). However, the significant advantages of the adsorption technique are its high efficiency in removing very low levels of heavy metals from dilute solutions, easy handling, high selectivity, lower operating cost, minimization of chemical or biological sludge, and regeneration of the adsorbent (Ozdes et al., 2011). This is why materials and structures such as nanoparticles (NPs) as alternative low-cost adsorbents are being paid considerable attention.

Currently NPs are used in wide range of applications, including shape selective catalysis, chromatographic separations, sorption of metal ions, enzyme encapsulation, in the fields of biotechnology and biomedicine for cell labeling and separation, magnetic resonance imaging (MRI), enzyme and protein separations, targeted drug delivery and magnetic ferrous fluids hyperthermia. To date, many technologies, mainly co-precipitation (Mahdavian and Mirrahimi, 2010), microemulsion (Drmota et al., 2012), thermal decomposition (Sharma and Jeevanandam,2012), hydrothermal synthesis (Xin, 2012), microwave assisted (Ahmed et al., 2013), sol-gel (Huang and Hu, 2008) and sonochemical synthesis (Vijayakumar, 2000) has been applied and reviewed for the production of NPs.

Application of nanostructures as adsorbents is valid for their use in other applications, requires particle stabilization and/or surface functionalization for good dispersion, particles suspension stability and no agglomeration in liquid media. Such stabilizing agents should be economical and widely available.

The aim of the present work was to synthesize iron oxide nanoparticles (iron oxide NPs and iron oxide NPs with the incorporation of silica gel (SiO_2) particles (iron oxide NPs - SiO_2), and evaluate their performance for the adsorption of Cr (VI) ions in aqueous solutions. The SiO_2 gel was incorporated as a synergist to evaluate its contribution to the enhancement of adsorption since it is reported that the SiO_2 surface strongly binds Fe (III) and Cr (III) ions via surface complexation (Oh et al., 2007).

2. Materials and Methods

2.1. Materials

All chemicals and reagents used for the experiments were analytical grades. Ferric chloride hexahydrate ($FeCl_3.6H_2O$, 99%, Sigma Aldrich, USA), ammonia solution (NH_4OH, 25%), ferrous sulphate heptahydrate ($FeSO_4.7H_2O$, 98.8%, Sigma Aldrich, USA), general purpose silicon oxide gel (SiO_2, Silica AR™ 40 - 63 microns (230 - 400 Mesh), Macron Fine Chemicals, USA), absolute ethanol (CH_3OH, 99.8%, Lobachemie, India), potassium dichromate ($K_2Cr_2O_7$, 99.9%, Lobachemie, India), 1,5-diphenyl carbazide (1,5-DPC, $C_{13}H_{14}N_4O$, 98%, Lobachemie, India), nitric acid (HNO_3, Riedel Dehaen, Germany), sulfuric acid (H_2SO_4, Riedel Dehaen, Germany), and hydrochloric acid (HCl, 35%, from Riedel Dehaen, Germany).

2.2. Methods

2.2.1. Preparation of the nanoparticles

2.2.1.1. Preparation of iron oxide NPs

The iron oxide NPs were synthesized by modification of a co-precipitation method (Sharma et al., 2009). In a typical experiment, the stoichiometric ratio 1:2 between the iron species, ferrous/ferric ions (Fe^{2+}/Fe^{3+}) was maintained. 6.0 g of $FeCl_3.6H_2O$ and 3.0 g of $FeSO_4.7H_2O$ were dissolved in 100 ml distilled water with stirring for 3 minutes at 2000 rpm. After 3 minutes, 25 ml NH_4OH 25% (precipitating agent) was added drop wise in 5-7 minutes. The reaction was continued for a further 30 minutes at a temperature of 90ºC; and the pH was maintained between 8 and 12 till a dark colored precipitate was formed. After stopping the reaction and magnetic field application, the reaction mass separated out into two phases: a clear aqueous phase on top and the consolidated precipitate at the bottom of the reaction vessel. The clear aqueous top phase was decanted and the black colored precipitate isolated by repeatedly washing with distilled water and centrifuging to remove excess chloride, sulphate ions and NH_4OH until the supernatant became neutral (pH~7.0). The precipitate was further washed with C_2H_5OH and dried at 150°C for 2 hours to obtain the iron oxide NPs.

2.2.1.2. Preparation of iron oxide NPs-SiO_2

1.5 ml (3 mol l^{-1}) HCl solution was added into 13 g l^{-1}aqueous SiO_2 gel suspension and stirred for 2 hours. After 2 hours, 50 ml serum was withdrawn and centrifuged, and the acid washed SiO_2 gel neutralized (Li et al., 2011). Thereafter, the SiO_2 gel was added to a 100 ml aqueous solution of 6 g of $FeCl_3.6H_2O$ and 3 g of $FeSO_4.7H_2O$ while stirring at 2000 rpm. After 3 minutes of stirring, 25 ml NH_4OH 25% (precipitating agent) was added drop wise in 5-7 minutes. The reaction was continued for a further 30 minutes at a temperature of 90ºC and the pH was adjusted till a dark colored precipitate was formed. After stopping the reaction and magnetic field application, the reaction mass separated out into a clear aqueous top phase and the consolidated black colored precipitate at the bottom of the reaction vessel. The clear aqueous top phase was decanted and the black colored precipitate repeatedly washed by distilled water and centrifuged to remove excess NH_4OH till the pH of the supernatant became neutral (pH~7.0). The centrifuged NPs were washed with C_2H_5OH and dried at 150^{o}C for 2 hours to obtain the iron oxide NPs-SiO_2.

2.3. Characterization

2.3.1. X-Ray diffraction analysis (XRD)

Phase analysis of the iron oxide NPs and iron oxide NPs-SiO_2 adsorbents was carried out by X-ray diffractometer (Model 7000S, Schimadzu Corporation, Japan), equipped with a Cu-Kα radiation (λ=1.5406 Å) source using a nickel filter and continuous scan mode in the range $10º < 2\theta < 80º$. The crystalline sizes of the iron oxide NPs and iron oxide NPs-SiO_2 adsorbents were determined using the Debye-Scherer's equation (1).

$$d = \frac{(0.94\lambda)}{\beta cos\theta} \quad (1)$$

Where D is the average crystalline diameter, 0.94 is the Scherer's constant, λ is the X-ray wavelength, β is the line broadening at half the maximum intensity and θ is the Bragg's angle in degrees.

The lattice parameter 'a' and interplanar spacing d_{hkl} was determined by Bragg's equations (2) and (3)

$$d_{hkl} = \frac{\lambda}{2sin\theta} \quad (2)$$

$$d_{hkl} = \frac{a}{\sqrt{h2+k2+l2}} \quad (3)$$

2.3.2. Fourier transform infrared spectroscopy (FTIR)

FTIR spectra of the iron oxide NPs and iron oxide NPs-SiO_2 samples were recorded on a spectrophotometer equipped with a deuterium triglycine sulfate (DTGS) detector (Model Spectrum 65 FT-IR Spectrometer, Perkin Elmer USA). Each sample of 1-2 mg was thoroughly mixed with approximately 100 mg KBr powder and pressed into disks by a 10-ton hydraulic press at room temperature. The prepared disks were scanned in the range 4000 cm^{-1} to 500 cm^{-1} at a resolution of 4 cm^{-1}.

2.3.3. Adsorption experiments

2.3.3.1. Preparation of $K_2Cr_2O_7$ stock solution and standard working solutions

A standard stock solution of $K_2Cr_2O_7$ was prepared by dissolving 2.828 g $K_2Cr_2O_7$ in 1000 ml of distilled water. Standard working solutions of different

concentrations, 20, 40, 60 and 80 mg l^{-1} of $K_2Cr_2O_7$ were prepared from this stock solution by appropriate dilutions. The pH of the solutions was adjusted to the desired value by addition of 0.1M HCl or 0.1M NaOH as required.

2.3.3.2. Calibration graph for determination of residual concentration of Cr (VI) ions

A linear calibration graph (Figure 1) was obtained over the range 10, 20, 40, 60 and 80 mg l^{-1} of Cr (VI) ions on a UV-Vis spectrophotometer (Model T 80+, PG Instruments Ltd., UK) with 1cm quartz cells at a wavelength of 540 nm. A commonly used specific reagent for the spectrophotometric determination of Cr (VI) ions, 1, 5-DPC (0.5%) solution was added to the standard working solutions to generate a reddish-purple color. The 1, 5-DPC (0.5%) solution was prepared by dissolving 0.25 g l^{-1}, 5-DPC in 50 ml acetone. 6N H_2SO_4 solution was prepared by adding 8.33 ml H_2SO_4 (98%) into 50 ml distilled water to be used for pH adjustments at UV measurements. Each measurement was carried out after 5 minutes of addition of the 1, 5-DPC solution and completed within 20 minutes to avoid loss of color due to instability.

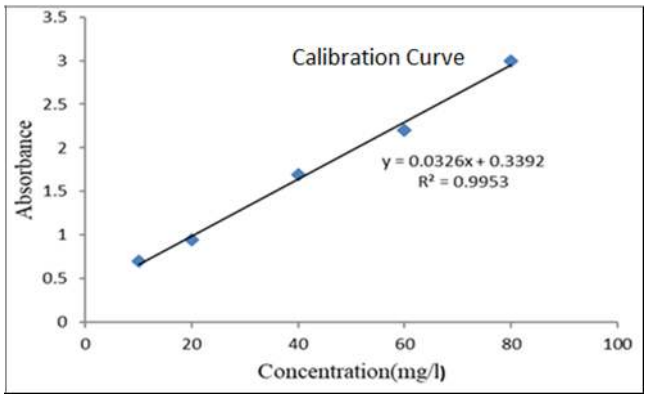

Figure 1: Calibration curve for Cr (VI)

2.3.3.3. Adsorption experiments

The parameters, initial Cr (VI) concentration (10, 20, 40, 60 and 80 mg l^{-1}), pH (2, 3, 4, 5, 6, 7, 8, 9 and 10), contact time (30, 45, 60, 90, 120 and 150 minutes) and adsorbent dosage (0.1, 0.2, 0.3, 0.4, 0.5, 0.6, 0.7 and 0.8 g l^{-1}) were chosen as independent variables and the removal efficiency of Cr (VI) ions as output response.

Two sets of batch adsorption experiments; one set using iron oxide NPs and the other using iron oxide NPs-SiO_2 as adsorbents were performed in 100 ml conical flasks containing 50 ml Cr (VI) ions working solutions and 0.1 g of the adsorbents. Both sets of mixtures were stirred on an orbital shaker at 100 rpm. After the predetermined times of contact, the adsorbents were removed from the sets of mixtures by a magnetic field and filtered. The adsorbent free solutions were then analyzed for residual Cr (VI) ions concentration by UV spectroscopy. Determination of Cr (VI) ions was performed by taking 40 ml of the solutions of the two sets in beakers and adding 3 ml of 6N H_2SO_4 to decrease the pH below 2. Once the pH was adjusted, 0.8 ml of 0.5% DPC solution was added to the solutions. After waiting for 5 minutes for stable color development, the UV measurements were performed. Percentage removal of Cr (VI) ions and amount of adsorption at equilibrium, q_e (mg g^{-1}), were calculated by using equations 4 and 5.

$$\text{Removal efficiency} = \frac{Co-Ce}{Co}\ x\ 100 \quad (4)$$

$$q_e = \frac{Co-Ce}{m}\ x\ V \quad (5)$$

Where C_o and C_e are the initial and final concentration of Cr (VI) ions (mg l^{-1}) in the solutions, respectively, V is the volume (*l*) of the tested solutions and m is the mass of the adsorbents (g) used.

2.3.4. Adsorption isotherms

The adsorption isotherms were analyzed using the Langmuir and Freundlich isotherm models.

3. Results and Discussion

3.1. Mechanism of iron oxide and SiO_2 supported iron oxide NPs formations

The reaction of Fe^{2+} and Fe^{3+} ions under alkaline conditions has been the subject of extensive investigation (Bandhu et al., 2009; Valenzuela et al., 2009; Gnanaprakash et al., 2007; Vereda et al., 2007).

The proposed mechanism, a dynamic equilibrium equation, put forth for the synthesis of Fe_3O_4 nanoparticles by the co-precipitation method (Mascolo et al., 2013) includes as the first reaction, a very fast precipitation of ferric and ferrous hydroxides:

$$Fe^{3+} + 3OH^- \rightleftharpoons Fe(OH)_3\ (s)$$

The second reaction, a slower one, involves decomposition of the ferric oxide to FeOOH:

$$Fe(OH)_3\ (s) \rightleftharpoons FeOOH\ (s) + H_2O$$

$Fe^{2+} + 2OH^- \rightleftharpoons Fe(OH)_2$ (s)

The third reaction, a solid state reaction, occurs between FeOOH and $Fe(OH)_2$ due to the low water activity of the solution to produce Fe_3O_4:

$2FeOOH$ (s) + $Fe(OH)_2$ (s) $\rightleftharpoons$ Fe_3O_4 (s) + $2H_2O$

The concentration and size of the Fe_3O_4 nanoparticles are influenced by the Fe^{3+}, Fe^{2+} and OH^- ions, as well as the water activity of the solution, with the overall reaction being:

$2Fe^{3+} + Fe^{2+} + 8OH^- \rightleftharpoons 2Fe(OH)_3Fe(OH)_2$ (s) $\rightarrow$ Fe_3O_4 (s) + $4H_2O$

The stoichiometry of Fe^{+2} to Fe^{3+} molar ratio, 1:2 used in this study is considered the stoichiometry for synthesis of high purity Fe_3O_4 NPs magnetite (Mascolo et al., 2013). The final [OH^-] concentration, related to the pH and base amount, controls the nucleation and growth of the Fe_3O_4 NPs influencing the particle size and saturation.

3.2 X-ray diffraction

Figure 2 (a and b) show the XRD patterns of the iron oxide NPs and iron oxide NPs-SiO_2 adsorbents. The diffraction patterns have well defined diffraction peaks, indicating that the samples were crystalline.

The apparent absence of lines 110 (d = 4.183Å) at 2θ = 21.22° and 104 (d = 2.700Å) at 2θ = 33.15° indicated that both goethite (α-FeOOH) and hematite (α-Fe_2O_3) were not formed. Peaks of $Fe(OH)_3$ (d = 3.376Å) at 2θ = 26.38° as well as other phases of iron oxide hydroxides, γ-FeO(OH) and δ-FeO(OH) were also not detected. The other two forms of iron oxide, magnetite (Fe_3O_4), and maghemite (γ-Fe_2O_3) have a spinel structure. Their lines being very close, makes it is very difficult to distinguish them from one another by X-ray diffraction. The color of the just synthesized iron oxide NPs was black in color indicating that the major form of iron oxide should be Fe_3O_4. The γ-Fe_2O_3 phase is known to exhibit a few extra peaks at 23.77° (210) and 26.10° (211), though with weak intensities (Kim et al., 2012). Based on the color and two extra typical peaks alone, it cannot be definitely ascertained whether the iron oxide NPs formed were pure Fe_3O_4 NPs as trace amounts of γ-Fe_2O_3NPs may probably be formed as contaminant during the co-precipitation processes. γ-Fe_2O_3 NPs are orange red to brown in color and very different from black color Fe_3O_4, but when present in trace amounts in a Fe_3O_4 NPs sample it is not possible to distinguish it by color.

A comparison of the XRD patterns of the prepared iron oxide NPs and iron oxide NPs-SiO_2 adsorbents (Figure 2a and b) after washing and drying with the patterns of pure commercial Fe_3O_4 NPs (Sigma–Aldrich 310069*)* and γ-Fe_2O_3 NPs (Sigma–Aldrich 544884*)* (Figure 3a and b) (Kim et al., 2012) shows that the synthesized adsorbents display the characteristic (210) and (211) peaks indicating the presence of the γ-Fe_2O_3 phase. The transition of the Fe_3O_4 NPs phase to the γ-Fe_2O_3 phase in the adsorbents is attributed to the oxidation process initiated during the iron oxide NPs synthesis, drying at elevated temperature of 150°C and subsequent storage in air prior to characterization and further use for the Cr (VI) ions adsorption experiments. There was a marked change in color observed from the initial black color of the just synthesized iron oxide NPs prior to drying to red brown after drying and storage. It has been shown that fine size Fe_3O_4 crystals (e.g., 10-20 nm) rapidly undergo transition to γ-Fe_2O_3 at around 150°C, whereas the larger Fe_3O_4 particles were more thermally stable and did not start the transition to γ-Fe_2O_3 until about 315°C (Lauer Jr. et al., 2001).The obtained XRD patterns and visual color observations made are in agreement. The series of characteristic diffraction peaks observed in the XRD patterns of the adsorbents (Figure 2(a and b)) at 2θ of 30.2°, 35.5°, 43.2°, 53.6°, 57.3° and 63° are indexed as (220), (311), (400), (422), (440), and (511) crystal planes correspond to a cubic unit cell of Fe_3O_4, and match the inverse-spine structure. The peaks correspond to maghemite phase (210) and (211) also observed in Fe_3O_4-SiO_2 phase due to the transition of Fe_3O_4 NPs to γ-Fe_2O_3.

The diffraction peaks of the iron oxide NPs-SiO_2 adsorbent (Figure 2b) were marginally broader than those of the iron oxide NPs adsorbent, which indicated the presence of a still finer nature and smaller crystallite size of the NPs in the former. In addition, the pattern showed the peaks for SiO_2. The SiO_2 was of the crystalline form since the broad peak at the 2θ value of 22°, a characteristic of SiO_2 in the amorphous form was absent. The sharp XRD peaks at 2θ values of 20.81, 26.49 and 50.1 (overlapped by the contribution from the iron oxide NPs) indicated that SiO_2 was in the crystalline form (Saceda et al., 2011).

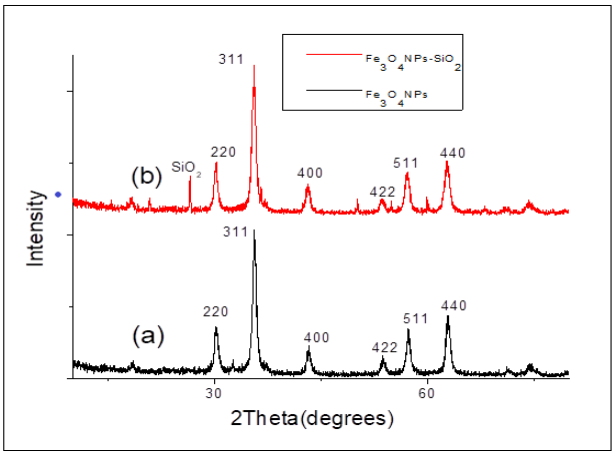

Figure 2: X-ray diffraction patterns of (a) iron oxide NPs and (b) iron oxide NPs-SiO_2.

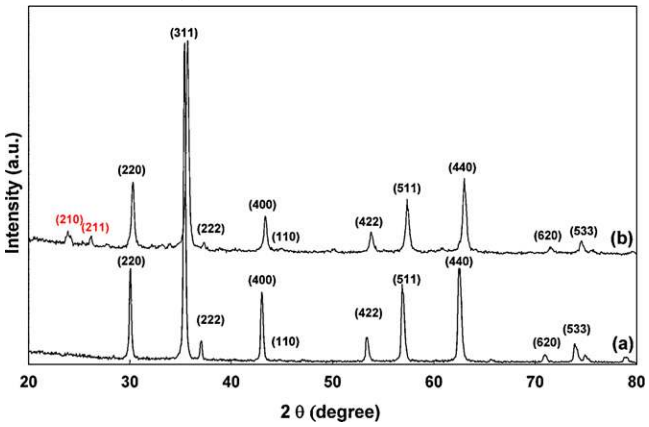

Figure 3. X-ray diffraction patterns of commercial powders (a) magnetite (Fe_3O_4), Sigma–Aldrich 310069 (b) maghemite (γ-Fe_2O_3), Sigma–Aldrich 544884.The characteristic (210) and (211) peaks of the maghemite phase are obvious.

The calculated crystal size of the iron oxide NPs and iron oxide NPs-SiO_2 adsorbents were 13.5 nm and 12.8 nm respectively and in close approximation. These particle sizes confirm the capping of Fe_3O_4 with SiO_2 from growth and agglomeration.

The Fe_3O_4 phase transition to γ-Fe_2O_3 NPs is due to oxidation of Fe (II) to Fe (III). This transition takes place at relatively low temperatures, even at room temperature, in ultrafine Fe_3O_4 NPs due to the exposed large surface area of Fe_3O_4. Once oxidation is initiated it tends to go to completion within the particles (Haneda and Morrish, 1977).

The lattice parameters of Fe_3O_4 and γ-Fe_2O_3 phases are very close and difficult to be differentiated unless it is a single phase of well-crystallized structure. The calculated lattice parameters (Table 1) for the iron oxide NPs and iron oxide NPs-SiO_2 adsorbents were 8.3504°A and 8.373°A respectively and lie in between those of commercial Fe_3O_4 (8.396 ˚A [JCPDS 19-629]) and γ-Fe_2O_3 (8.3515Å [JCPDS 39-1346] (Kim et al., 2012). These values affirm silica supported iron oxide NPs adsorbents that prepared were a mixture of Fe_3O_4 and γ-Fe_2O_3 phases.

The interplanar spacing for the iron oxide NPs and iron oxide NPs-SiO_2 adsorbents are lower than the values reported for bulk magnetite (JCPDS Card No. (79-0417)) [d_{311}= 2.531]) (Ghandooret al., 2012) and are attributed to the formation of γ- Fe_2O_3 (a = 8.347 and d_{311}=2.517) (Victoria et al., 2007; Cornell and Schwertmann 2003).

Table1: Interplanar spacing, Lattice parameters of iron oxide NPs and iron oxide NPs –SiO_2

Sample	**Calculated particle size**	**Interplanar spacing D_{hkl} (Å)**	**Lattice parameter 'a' (Å)**
Iron oxide NPs	13.5 nm	2.51774	8.3504
Iron oxide NPs- SiO_2	12.8 nm	2.52463	8.373
Magnetite (Fe_3O_4) Sigma–Aldrich No.310069	1 µm	-	8.396 (JCPDS 19-629)
Maghemite (γ-Fe_2O_3) Sigma–Aldrich No. 544884	<50 nm	-	8.3515 (JCPDS39-1346)

3.3 FTIR Analysis

Figures 4 (a & b) show the FTIR spectra of the iron oxide NPs and iron oxide-SiO_2 NPs respectively after drying at 150°C. In both spectra, the broad band in the proximity of 3400 – 3412 cm^{-1} and at 1634 cm^{-1} are attributed to the stretching vibration of the O-H groups on the surface of the NPs (Petcharoen and Sirivat, 2012; Haw et al., 2011) and or to adsorbed water on the surface. A third expected vibration, however, from condensed octahedral Fe_2O_6 at 390cm^{-1}) (Jitianu, et al., 2006) could not be identified due to the scanning range limitation. The band at 1119 cm^{-1} is attributed to the Fe-OH bond due to octahedral sites of the Fe_3O_4.

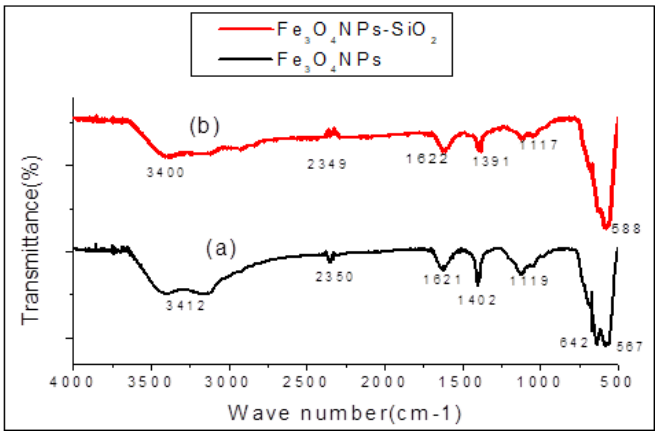

Figure 4: FT-IR spectra of (a) iron oxide NPs and (b) iron oxide NPs-SiO_2.

A sharp peak at 2360 cm^{-1} is the CO_2 vibration (Banerjee and Chen, 2007). The band observed in the region of 567 cm^{-1} to 588 cm^{-1} with a shoulder in the proximity700 cm^{-1} is attributed to presence of Fe_3O_4 (Sun et al., 2009). This band overlaps a characteristic band of γ-Fe_2O_3 at 582 cm^{-1} and the distinct high-frequency shoulder in the proximity of 635 cm^{-1} to 642 cm^{-1} is also characteristic to γ-Fe_2O_3 (Fu et al., 2008). Both these bands correspond to the ν(Fe-O) deformations in the tetrahedral and the octahedral sites. Further, as seen from Figure 4b, the weak bands between 800 and 1260 cm^{-1} are ascribed as a superimposition of various SiO_2 peaks and Si–OH bonding (Vasconcelos et al., 2002).

3.4. Factors Affecting Chromium Adsorption

3.4.1 Effect of initial Cr (VI) ion concentration on adsorption

Standard working solutions with Cr (VI) ions concentration of 20, 40, 60 and 80 mg l^{-1} and optimal pH 3 were equilibrated for 120 minutes using an absorbent dose of 0.7g l^{-1}at room temperature. Figure 5 shows that the Cr (VI) ions removal efficiency of the absorbent iron oxide NPs-SiO_2 was higher than that of the adsorbent iron oxide NPs at all concentrations. The decrease in adsorption efficiencies of the iron oxide NPs and iron oxide NPs-SiO_2 with increasing standard working solution concentration ranged from 74% to 39% and 97.4% to 55% respectively. At low initial concentrations, the ratio of the initial number of Cr (VI) ions to the accessible active sites of the adsorbents will be low with the reverse occurring at higher initial concentration. Thus, the removal efficiency of Cr (VI) is higher at lower Cr concentration and lower at higher concentrations with further residual Cr (VI) ions remaining in the aqueous solutions (Radnia et al., 2012).

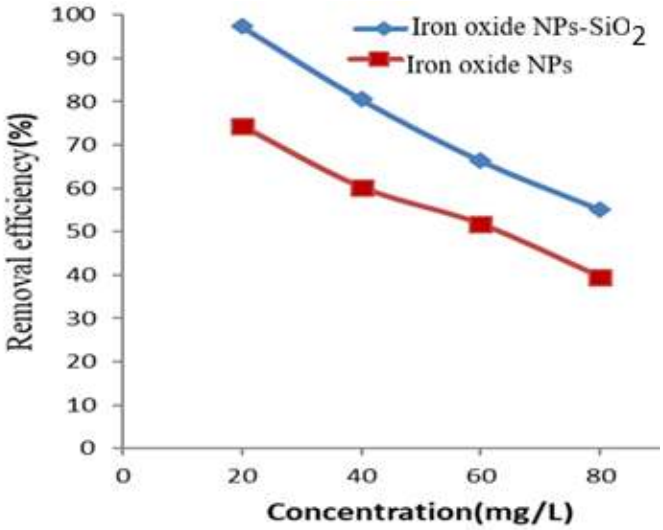

Figure 5. Effect of initial concentration of Cr (VI) on removal efficiency of iron oxide NPs and iron oxide NPs-SiO_2 (C_0 = 10–100 mg l^{-1}, pH = 3, adsorbent dose = 0.7 g l^{-1}, contact time = 120 minutes and room temperature).

The higher removal efficiency by the iron oxide NPs-SiO_2 adsorbent in comparison to the iron oxide NPs is attributed to the presence of SiO_2 gel. In the adsorption process, factors which influence the capacity of the silica for the removal of Cr (VI) from aqueous solutions include the structural texture and characteristics of the gel particles such as surface area, porosity, and the availability of surface silanols. For example, it is reported that SiO_2 gels because of having high surface area, high mass exchange characteristics, and

availability of high siliceous surfaces, are the mostly utilized substrates to be modified for the removal of toxic metal ions (Jal et al., 2004). At the same time, it has been shown that the surface of SiO_2 strongly binds Fe (III) and Cr (III) via surface complexation (Fendorf et al., 1994; Flogeac et al., 2005; Oh et al., 2007). Thus, it is reasonable to presume that the silica gel present in Fe_3O_4-SiO_2 provides sites for adsorption of Fe (III), Cr (III), and other reaction precipitates such as Fe (III)-hydroxides and Cr (III)/Fe (III) hydroxides. This would lead to more free binding sites for Cr (VI) on the iron oxide NPs.

Another contributing factor is the smaller size of the iron oxide NPs in the iron oxide NPs-SiO_2 adsorbents as deduced by XRD analysis resulting in large surface area and binding sites available for adsorption.

Based on the enhanced performance of the adsorbent iron oxide NPs-SiO_2 adsorbent compared that of the adsorbent iron oxide NPs for the removal of Cr (VI), other factors such as pH, adsorbent dose and contact time that affect the adsorption behavior were evaluated only for the iron oxide NPs-SiO_2 adsorbent.

3.4.2. Effect of pH on the adsorption of Cr (VI) ions

The aqueous pH significantly modifies heavy metals adsorption, influencing surface chemistry (Chowdhury et al., 2012), determining the adsorbent surface charge and the degree of ionization and speciation of the adsorbed species (Al-Qodah, 2006; Ahmed et al., 2013; Badr and Al-Qahtani, 2013). In general, the surfaces of metal oxides are covered with hydroxyl (OH) groups that vary in form at different pH levels. These groups, either from the adsorption of water or from structural attributes, are the functional groups of iron oxides. The groups have a double pair of electrons together with a dissociable hydrogen atom which can help them to react with both acids and bases. Charge on iron oxide surfaces is generated by the dissociation (ionization) of these OH groups. This results in the adsorption or desorption of protons depending on the pH of the solution.

The effect of pH on the adsorption of Cr from the standard working solutions containing 20, 40 and 60 mg l^{-1} Cr (VI) was evaluated only for the iron oxide NPs-SiO_2 adsorbent at a dose of 0.7 g l^{-1} and 120 minutes contact time (Figure 6). Maximum Cr removal efficiency obtained was 96.5, 88 and 80% respectively at pH 3 from the above standard working solutions. The efficiency increased sharply between pH 2-3 from 57.7% to 96.5%, then decreased rapidly to 50.5% with an increase in pH from 3 to 7 and then tapered sharply to 45% with a further increase in pH between 7 and 9. Since the iron oxide NPs-SiO_2 adsorbent is a mixed form of maghemite–magnetite, the acidity constants of a specific surface group will depend on the abundance of Fe^{2+}or Fe^{3+} and its hydrolysis products. The dominant functional groups of most iron oxide surfaces are expected to be Fe^{2+} or $FeOH^{+}$ when the solution pH is acidic; and $Fe(OH)_2^0$ and $Fe(OH)_3^-$ when the solution pH is basic. The high Cr (VI)ions adsorption observed in the lower pH acidic range is due to the iron oxide NPs surface having a net positive charge form Fe-OH_2^+ surface groups. At low pH, the different Cr anionic species ($Cr_2O_7^{2-}$, $HCrO_4^-$, $Cr_3O_{10}^{2-}$, $Cr_4O_{13}^{2-}$) coexist in water (Yuan et al., 2009). At pH 2–3, $HCrO_4^-$ is favorably adsorbed due to its low adsorption free energy (−2.5 to−0.6 kcal/mol) (Chowdhury et al., 2012).

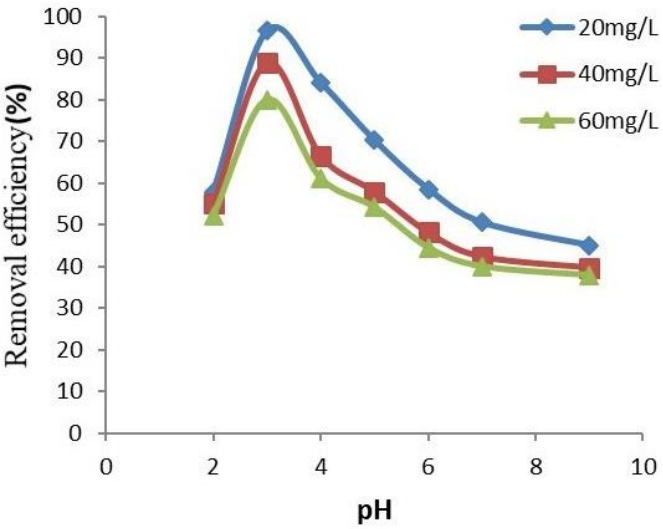

Figure 6: Effect of initial pH on removal efficiency by iron oxide NPs-SiO_2 (C_0 = 20, 40 and 60 mg l^{-1}, adsorbent dose = 0.7 g l^{-1} and contact time = 120 minutes).

At higher pH, the surface OH groups on the iron oxide NP surface are $Fe(OH)_2^0$ and $Fe(OH)_3^-$. Because of this negative surface charge of iron oxide, the surface will repel the negatively charged Cr (VI) ion species at higher pH values. Fe(III) in solution (from maghemite) will form hydrated ferric oxides (HFO) NPs. Adsorption keeps the Cr (VI) ions on the iron oxide surfaces through Lewis acid base interactions wherein the surface Fe atoms are Lewis acids that react with Lewis bases (e.g.,

water). The surface OH groups of the iron oxides are the chemically reactive entities at the surface of the solid in an aqueous environment possessing a double pair of electrons that enables them to react with acid and bases (Chowdhury et al., 2012).

3.4.3. Effect of adsorbent dose on Cr (VI) ions removal

The effect of the dose of iron oxide NPs-SiO_2 adsorbent in the range of 0.1 g l^{-1} to 0.8 g l^{-1} on the removal of Cr (VI) ions from the standard working solutions of Cr (VI) concentration 20 and 40 mg l^{-1}, at pH 3 for 120 minutes contact time is shown in Figure 7. From the figure it is observed that the percentage removal of Cr (VI) ions increased from 58 to 96.4% and from 52% to 85% for the working standard solutions of Cr (VI) concentration 20 and 40 mg l^{-1} respectively with increasing amount of adsorbent dose till 0.7gl^{-1} beyond which it saturated. This is explained by the increase of effective surface area on which metal ions will be adsorbed with absorbent dose, meaning that increasing the adsorbent dose will result in an increase in the number of active sites available for adsorption (Sharma et al., 2009).On the other hand, this will result in a continual decrease of the adsorption capacity with increase of adsorbent dose and this situation is a result of remaining of effective surface area without saturation along with the adsorption process. Similar results have been observed in the other seminal studies using different adsorbents for the removal of Cr (VI) (Li et al., 2008).

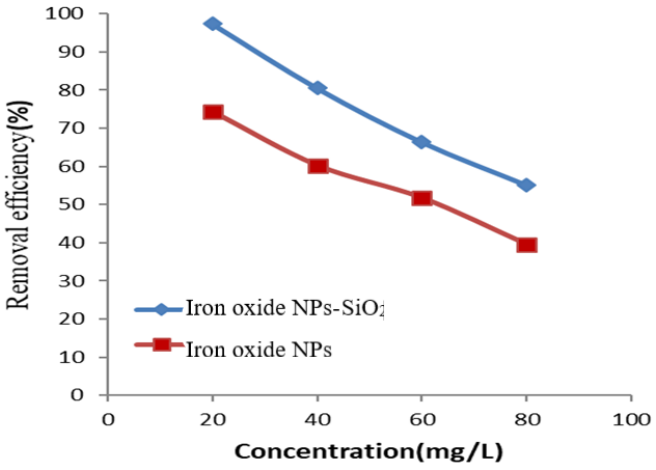

Figure 7: Effect of adsorbent dose on removal efficiency by iron oxide NPs-SiO_2 (C_0 = 20 and 40 mg l^{-1}, pH = 3, contact time = 120 minutes, and room temperature).

At an adsorbent dose of 0.8 g l^{-1}, the percentage removal is 95 and 84.5% for the standard working Cr (VI) solutions of concentration 20 and 40 mg l^{-1} respectively which is marginally lower by ~1.5 and 0.5% compared to the percentage removal at an adsorbent dose of 0.7 g l^{-1}.Thus, under the given experimental conditions, a 0.7 g l^{-1} adsorbent dose is deemed optimal for maximum percentage Cr (VI) ions removal.

3.4.4. Effect of contact time on the adsorption of Cr (VI)

The rates of Cr (VI) ions removal from three standard solutions with initial Cr concentration of 20, 40 and 60 mg l^{-1} at pH 3 using a fixed iron oxide NPs-SiO_2 adsorbent dose of 0.7 g l^{-1} and contact time ranging from 25 to 150 minutes at room temperature are shown in Figure 8. From the figure, it is observed that adsorption equilibrium was achieved in 120 minutes beyond which it remained constant to 150 minutes. The rapid metal uptake by the adsorbent in majority is attributed to adsorption on the external surfaces of the iron oxide nanoparticles where almost all of the sorption sites exist as well on the SiO_2 gel particles. Any contribution by micro-porous adsorption is essentially expected from the SiO_2 gel particles.

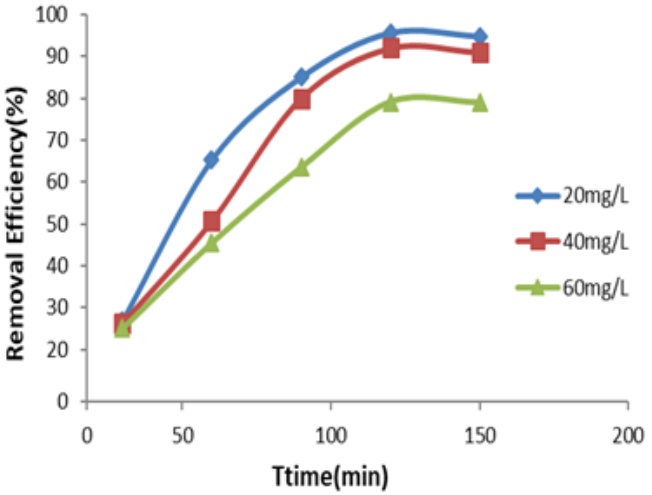

Figure 8: Effect of contact time on removal efficiency (C_0 =20, 40 and 60 mg l^{-1}, T = 25°C, adsorbent iron oxide NPs-SiO_2 dose = 0.7 g l^{-1}, pH = 3, and room temperature).

Thus, it is easy for the Cr (VI) ions to access these active sites, resulting in a rapid approach to equilibrium. A two-step fundamental mechanism of Cr (VI) ions adsorption onto the iron oxide NPs-SiO_2 can be

expected. In a first step, Cr (VI) ions will migrate from the bulk solution phase to the outer particle surfaces of the adsorbent and establish contact (film diffusion). In the second, electrostatic attraction or reactions occurring between adsorbate Cr (VI) ions and adsorbent will take place (Singh et al., 1993).

3.5 Adsorption Isotherms

In this work because of the better performance of the adsorbent iron oxide NPs-SiO2, the adsorption isotherms of this adsorbent were analyzed only.

The equilibrium adsorption isotherm model is the number of mg adsorbed per g of an adsorbent (q_e) vs. the equilibrium concentration of adsorbate and provides a fundamental description of the interaction between an adsorbate and an adsorbent. The analysis data allows for predicting the adsorption capacity of the adsorbent, a main parameter required for the design of an adsorption system. Equilibrium isotherm studies were carried out with different initial concentrations of Cr(mg l^{-1}) at room temperature and pH 3.The equilibrium adsorption data were analyzed by Langmuir's model (Langmuir, 1918) and Freundlich's model (Freundlich and Heller, 1939).

Langmuir's model, based on the physical hypothesis that: the maximum adsorption capacity consists of a monolayer adsorption, that there are no interactions between adsorbed molecules, and that the adsorption energy is distributed homogeneously over the entire coverage surface, essentially provides the simplest description of the adsorption process without taking into account the variation in adsorption energy (Chatterjee et al., 2009; Afkhami et al., 2009).

The isotherm is represented by

$$\frac{C_e}{q_e} = \frac{K_L C_e}{Q_m} + \frac{1}{Q_m} \quad (6)$$

Where C_e (mg/l) is the concentration of adsorbate left in solution at equilibrium, K_L is the Langmuir bonding energy, Q_m(mg g^{-1}) is the adsorption maximum (mg g^{-1}) and q_e(mg g^{-1}) is the amount of adsorbate adsorbed per unit mass of adsorbent.

The Langmuir constants Q_m and K_L were determined from the intercept and slope of the linear plot of C_e/q_e, against the equilibrium concentration C_e (mg l^{-1}) (Figure 9).

The Freundlich isotherm model, an empirical equation, describes the surface heterogeneity of the sorbent while considering multilayer adsorption with a heterogeneous energetic distribution of active sites, accompanied by interactions between adsorbed molecules (Chatterjee et al., 2009). The linearized form of the Freundlich adsorption isotherm equation is

$$\ln q_e = \ln k_f + \frac{1}{n}(\ln C_e) \quad (7)$$

Where q_e is the amount of adsorbate absorbed at equilibrium (mg g^{-1}), C_e is the equilibrium concentration of adsorbate in solution (mg l^{-1}), and the Freundlich constants (temperature dependent and the given adsorbent–adsorbate couple) K_f ($mg^{1-1/n} l^{1/n}\ g^{-1}$) is the capacity of the adsorbent (mgg^{-1}) and $1/n$ (lm g^{-1}) is related to the adsorption energy distribution. When the value of n is 1, the adsorption is a linear isotherm. If the value of n is less than 1 or greater than 1, it implies that the adsorption reaction is related to a chemical or favorable physical process, respectively. From Table 2, the value of n is greater than 1, indicating favorable adsorption and confirming that adsorption is a physical process.

The values of K_f and $1/n$ calculated from the intercept and slope of the plot of ln q_e vs. ln C_e (Figure 10) are shown in Table 1 wherein it is observed that the values of the correlation coefficient, R^2, for the fit of the experimental isotherm data to Langmuir equation is more close to 1 than that for the Freundlich equation. Therefore, the Langmuir model represents the experimental data better on the basis of values of regression coefficients. The agreement of the experimental results with the Langmuir model suggests monolayer coverage of Cr (VI) ions mainly on the outer surface of the adsorbent (Gholipour et al., 2011).

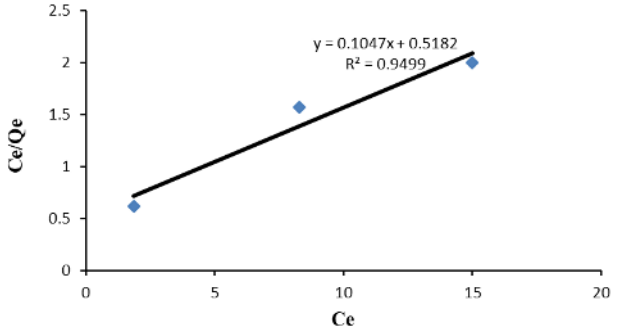

Figure 9: Linearization of the Langmuir isotherm (pH = 3, iron oxide NPs-SiO_2 = 0.7 g, room temperature)

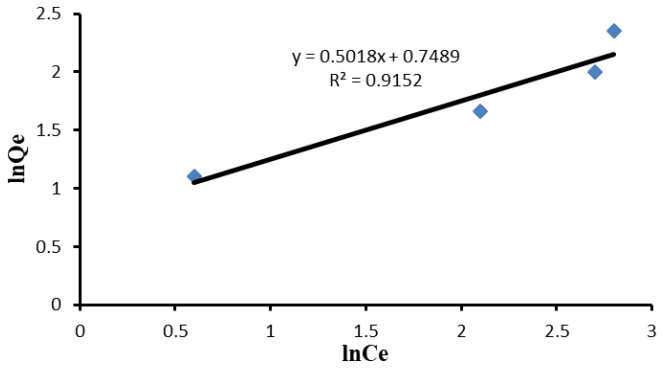

Figure 10: Linearized Freundlich isotherm (pH = 3, iron oxide NPs-SiO_2= 0.7 g, room temperature).

Table 2: Parameters of Langmuir and Freundlich isotherm equations, regression coefficients (r) for the adsorption of Cr (VI) ions on the iron oxide NPs-SiO_2 absorbent at room temperature and pH = 3.

Equation	Correlation coefficient (R^2)	Calculated isotherm parameters
Langmuir	0.9499	Q_m(mg g^{-1})=1.93, K_L(l mg^{-1}) = 0.20
Ferundlich	0.9152	K_f = 2.11, n = 1.335

4. Conclusion

The synthesized adsorbents, iron oxide NPs and iron oxide NPs-SiO_2, are mixed oxides of Fe_3O_4-γ-Fe_2O_3 of ultrafine particle size as evidenced by color change, XRD and FTIR analysis.

At room temperature, the performance of the adsorbent iron oxide NPs-SiO_2 for the removal of Cr (VI) from aqueous solutions was superior to that of the adsorbent iron oxide NPs vis-à-vis the initial concentration of Cr (VI)with maximum adsorption capacity at pH 3. This evidenced that the incorporation of a small amount of SiO_2 gel in the iron oxide NPs was synergistic. The removal of Cr (VI) from aqueous solutions by the adsorbent iron oxide NPs-SiO_2 at room temperature showed a strong dependency on the pH of the solution, adsorbent dosage, initial Cr (VI) concentration and contact time. An increase in the adsorbent iron oxide NPs-SiO_2 dose and decrease in the initial concentration of Cr (VI) resulted in an increase in Cr (VI) adsorption, while an increase in contact time lead to an increase in the removal of Cr (VI). The analysis of adsorption isotherms for the adsorbent iron oxide NPs-SiO_2 by the Langmuir and Freundlich adsorption isotherms showed that the Langmuir isotherm had a better fitting model than Freundlich as the former had a higher correlation regression coefficient. This indicated the applicability of monolayer coverage of the Cr (VI) on the surface of the adsorbent. Thus, the overall results showed that no rigorous conditions are required for the synthesis of the adsorbents and the inclusion of a relatively low cost SiO_2 gel along with the adsorbent could be economically viable for the effective removal of Cr (VI) in aqueous solutions.

Reference

Acar, F. N. and Malkoc, E. (2004). The removal of chromium (VI) from aqueous solutions by Fagus orientalis, L. *Bioresource and Technol*ogy, *94*: 13–15.

Afkhami, A., Madrakian, T. and Amini, A. (2009). Mo(VI) and W(VI) Removal from water samples by acid-treated high area carbon cloth. *Desalination, 243*: 258–264.

Ahmed, M.A., Ali, S.M., El-Dek, S.I. and Galal, A. (2013). Magnetite–hematite nanoparticles prepared by green methods for heavy metal ions removal from water. *Materials Science and Engineering: B*, *178*(10): 744-751.

Ahmed, M. J. K. and Ahmaruzzaman, M. (2016). A review on potential usage of industrial wastematerials for binding heavy metal ions from aqueous solutions. *Journal of Water Processing and Engineering, 10*: 39–47.

Al-Qodah, Z. (2006). Biosorption of heavy metal ions from aqueous solutions by activated sludge. *Desalination*, *196*(1-3): 164-176.

Badr, N. and Al-Qahtani, K.M. (2013). Treatment of wastewater containing arsenic using Rhazya stricta as anew adsorbent. *Environmental monitoring and assessment*, *185*(12): 9669-9681.

Bandhu, A., Mukherjee, S., Acharya, S., Modak, S., Brahma, S.K., Das, D. and Chakrabarti,P.K.(2009). Dynamic magnetic behaviour and Mössbauer effect measurements of magnetite nanoparticles prepared by a new technique in the co-precipitation method. *Solid State Communication*, *149*: 1790–1794.

Banerjee, S.S. and Chen, D.H. (2007). Fast removal of copper ions by gum arabic modified magnetic nano-adsorbent. *Journal of Hazardous Materials, 147*(3): 792-799.

Boyd, R. S. (2010). Heavy metal pollutants and chemical ecology: exploring new frontiers. *Journal of Chemical Ecology, 36*: 46–58.

Chatterjee, S., Lee, D.S., Lee, M.W. and Woo, S.H. (2009). Enhanced adsorption of congo red from aqueous solutions by chitosan hydrogel beads impregnated with cetyl trimethyl ammonium bromide. *Bio resource and Technology*, *100*: 2803–2809.

Cheng S. (2003). Effects of heavy metals on plants and resistance mechanisms. *Environmental Science and Pollution Reseach International. 10*(4): 256-264.

Chowdhury, S.R., Yanful, E.K. and Pratt, A.R. (2012). Chemical states in XPS and Raman analysis during removal of Cr (VI) from contaminated water by mixed maghemite–magnetite nanoparticles. *Journal of Hazardous Materials, 235*: 246-256.

Cornell, R.M. and Schwertman, U. (2003). *The iron oxides: structure, properties, reactions, occurrences and uses*. John Wiley & Sons.

Drmota, A., Koselj, J. and Žnidaršič, A. (2012). Microemulsion method for synthesis of magnetic oxide nanoparticles. *Intech open science/open minds,* 192-214.

Duruibe, J.O., Ogwuegbu, M.O. C. and Egwurugwu, J. N. (2007). Heavy metal pollution and human biotoxic effects. *International Journal of Physical Sciences, 2*(5): 112-118.

Farimani, M.H.R., Shahtahmasebi, N., Roknabadi, M.R., Ghows, N. and Kazemi, A. (2013). Study of structural and magnetic properties of superparamagnetic Fe_3O_4/SiO_2core–shell nanocomposites synthesized with hydrophilic citrate-modified fe_3o_4 seeds via a sol-gel approach. *Physical E: Low-Dimensional.*

Flogeac, K., Guillon, E. and Aplincourt, M. (2005). Adsorption of several metal ions onto a model soil sample: equilibrium and EPR studies. *Journal of Colloidal Interface Science*, *286*: 596–601.

Freundlich, H. and Heller, W. (1939). The adsorption of cis- and trans-azobenzene. *Journal of American Chemical Society , 61*: 2228–2230.

Fu, R., Wang, W., Han, R. and Chen, K. (2008). Preparation and characterization of γ-Fe_2O_3/ZnO composite particles. *Materials Letters*, *62*(25): 4066-4068.

Ghandoor. H.E.l., Zidan H. M., Mostafa. M.H., Khalil and IsmailM. I. M. (2012). Synthesis and some physical properties of magnetite(Fe_3O_4) nanoparticles. *International Journal of Electrochemistry and Science,* **7**: 5734 - 5745.

Gholipour, M., Hashemipour, H. and Mollashahi, M. (2011). Hexavalent chromium removal from aqueous solution via adsorption on granular activated carbon: adsorption, desorption, modeling and simulation studies. *Journal of Engineering and Applied Science*, *6*(9): 10-18.

Gnanaprakash, G., Philip, J., Jayakumar, T. and Raj, B. (2007). Effect of digestion time and alkali addition rate on physical properties of magnetite nanoparticles. *Journal of Physical. Chemistry, 111*:7978–7986.

Haneda, K. and Morrish, A. H. (1977). Magnetite to maghemite transformation in ultrafine particles. *Le Journal de Physique Colloques*. *38*(C1), C1-321.

Haw, C. Y., Chia, C. H., Zakaria, S., Mohamed, F., Radiman, S., Teh, C. H. and Huang, N. M. (2011). Morphological studies of randomized dispersion magnetite nanoclusters coated with silica. *Ceramics International*, *37*(2): 451-464.

Huang, C. and Hu, B. (2008). Silica-coated magnetic nanoparticles modified with γ-mercaptopropyltrimethoxysilane for fast and selective solid phase extraction of trace amounts of Cd, Cu, Hg, and Pb in environmental and biological samples prior to their determination by ICPM. *Spectrochimica Acta Part B, 63*(3): 437-444.

Jal, P. K., Patel, S. and Mishra, B. K. (2004). Chemical modification of silica surface by immobilization of functional groups for extractive concentration of metal ions. *Talanta, 62*: 1005−1028.

Jitianu, A., Raileanu. M., Crisan. M., Predoi. D., Jitianu, M., Stanciu, L. and Zaharescu, M. (2006). Fe_3O_4–SiO_2nanocomposites obtained via alkoxide and colloidal route. *Journal of Sol-gel Science and Technology,40*(2-3): 317-323.

Kim, W., Suh, C. Y., Cho, S. W., Roh, K. M., Kwon, H., Song, K. and Shon, I. J. (2012). A new method for the identification and quantification of magnetite–maghemite mixture using conventional X-ray diffraction technique. *Talanta*, *94*: 348-352.

Kumar, V., Rana, A., Yadav, M.S. and Pant, R.P. (2008). Size-induced effect on nano-crystalline $CoFe_2O_4$. *Journal of Magnetism and Magnetic Materials, 320*(11): 1729-1734.

Kushwaha, O.S., Ver Avadhani, C., Tomer, N.S. and Singh, R.P. (2014). Accelerated degradation study of highly resistant polymer membranes for energy and environment applications. *Advances in Chemical Science,*3(2): 19-30.

Langmuir, L. (1918). The adsorption of gases on plane surfaces of glass, mica and platinum. *Journal of American. Chemical Society, 40*: 1361–1403.

Lauer Jr, H. V., Ming, D. W., Golden, D. C. and Lin, I. C. (2001). Characterization of the thermal properties of magnetite using differential scanning calorimetry. *In Lunar and Planetary Science Conference*, *32*.

Li, H., Li, Z., Liu, T., Xiao, X., Peng, Z. and Deng, L. (2008). A novel technology for biosorption and recovery hexavalent chromium in wastewater by bio-functional magnetic beads. *Bioresource Technology*, *99*(14): 6271-6279.

Li, Y., Li, T. andJin, Z. (2011). Stabilization of FeO nanoparticles with silica fume for enhanced transport and remediation of hexavalent chromium in water and soil. *Journal of Environmental Sciences*, *23*(7): 1211-1218.

Li, Y.S., Church, J.S. and Woodhead, A.L. (2012). Infrared and Raman spectroscopic studies on iron oxide magnetic nano-particles and their surface modifications. *Journal of Magnetism and Magnetic Material,324*(8): 1543-1550

Mahdavian, A. R. and Mirrahimi, M. A. S. (2010). Efficient separation of heavy metal cations by anchoring polyacrylic acid on superparamagnetic magnetite nanoparticles through surface modification. *Chemical Engineering Journal,159*(1-3): 264-271.

Mascolo, M., Pei, Y., and Ring, T. (2013). Room temperature co-precipitation synthesis of magnetite nanoparticles in a large pH window with different bases. *Materials*, *6*(12): 5549-5567.

Nadeem, M., Mahmood, A., Shahid, S. A., Shah, S. S., Khalid, A. M. and Mckay, G. (2006). Sorption of lead from aqueous solution by chemically modified carbon adsorbents. *Journal of Hazardous Materials,138*(3): 604-613.

NIOSH (National Institute for Occupational Safety and Health), Criteria for are commended standard (2013): occupational exposure to hexavalent chromium, department of health and human services, Centre for disease control and prevention, DHHS (NIOSH) Publication No. 128.

Odeh, L., Odeh, I., Khamis, M., Khatib, M., Qurie, M., Shakhsher, Z. and Qutob, M. (2015). Hexavalent chromium removal and reduction to Cr (III) by polystyrene tris (2-aminoethyl) amine. *American Journal of Analytical Chemistry*, *6*: 26-37

Oh, Y. J., Song, H., Shin, W. S., Choi, S. J. and Kim, Y. H. (2007). Effect of amorphous silica and silica sand on removal of chromium (VI) by zero-valent iron. *Chemosphere,66*: 858–865.

U.S. Department of Labor, Hexavalent chromium, OSHA (2009). 3373-10.

Ozdes, D., Duran, C. and Senturk, H. B. (2011). Adsorptive removal of Cd(ii) and Pb(ii) ions from aqueous solutions by using turkish illitic clay. *Environmental Management,92*: 3082-3090.

Petcharoen, K. and Sirivat, A. (2012). Synthesis and characterization of magnetite nanoparticles via the chemical co-precipitation method. *Materials Science and Engineering: B*. *177*(5): 421-427.

Radnia, H., Ghoreyshi, A.A., Younesi, H. and Najafpour, G.D. (2012). Adsorption of Fe (II) Ions from aqueous phase by chitosan adsorbent: equilibrium, kinetic and thermodynamic studies.*Desalination and Water Treatment, 50*(1-3): 348-359.

Saceda, J.J.F., Leon, R.L.D., Rintramee, K., Prayoonpokarach, S. and Wittayakun, J. (2011). Properties of silica from rice husk and rice husk ash and their utilization for zeolite y synthesis. *Quimica Nova, 34*(8), 1394-1397.

Saleh, T. A. (2017). Advanced nanomaterials for water engineering, treatment, and hydraulics. *IGI Global,* 1-384.

Sharma, B., Sarkar, A., Singh, P. and Singh, R. P. (2017). Agricultural utilization of biosolids: a review on potential effects on soil and plant grown. *Waste Management,64*: 117–132.

Sharma, G. and Jeevanandam. P. (2012). Single step thermal decomposition approach to prepare supported γ-Fe_2O_3nanoparticles. *Applied Surface Science*, *258*(8): 3679-3688.

Samarghandi, M. R., Asgari, G., Ahmadzadeh, A., Poormohammadi, A. and Ahmadian, M. (2015). Magnetite nanoparticles synthesis and modified with chitosan Fe_3O_4 biopolymers for removal of hexavalent chromium from aqueous solutions. *Journal of Chemical and Pharmaceutical Research*, *7*(4): 933-941.

Sharma Y.C., Srivastava V., Weng C.H. and Upadhyay S.N. (2009). Removal of Cr (VI) from wastewater by adsorption on iron nanoparticles. *The Canadian Journal of Chemical Engineering*, *87*(6): 921-9.

Singh, D.B., Gupta, G.S., Prasad, G. and Rupain war, D.C. (1993). The use of hematite for Cr (VI) removal. *Journal of Environmental. Science and Health A*, *28* (8): 1813–1826.

Singh, U. K. and Kumar, B. (2017). Pathways of heavy metals contamination and associated human health risk in Ajay river basin, India. C. *Chemosphere*, 1-174.

Smith, E. and Ghiassi, K. (2006). Chromate removal by an iron sorbent: mechanism and modeling. *Water Environment Research, 78*(1): 84-93.

Sun, X., Zheng, C., Zhang, F., Yang, Y., Wu, G., Yu, A. and Guan, N. (2009). Size-controlled synthesis of magnetite (Fe_3O_4) nanoparticles coated with glucose and gluconic acid from a single Fe (III) precursor by a sucrose bifunctional hydrothermal method. *The Journal of Physical Chemistry C*, *113*(36), 16002-16008.

Valenzuela, R., Fuentes, M.C., Parra, C., Baeza, J., Duran, N., Sharma, S.K., Knobel, M. and Freer, J. (2009). Influence of stirring velocity on the synthesis of magnetite nanopraticles (Fe_3O_4) by theco-precipitation method. *Journal of Alloys Compound*, *488,* 227–231.

Vasconcelos, D. C., Campos, W. R., Vasconcelos, V. and Vasconcelos, W. L. (2002). Influence of process parameters on the morphological evolution and fractal dimension of sol–gel colloidal silica particles. *Materials Science and Engineering: A*, *334*(1-2): 53-58.

Vereda, F., Vicente, J. and Hidalgo-Alvarez, R. (2007). Influence of a magnetic field in the formation of magnetite particles via two precipitation methods. Langmuir, *23*: 3581–3589.

Vijayakumar, R. (2000). Sonochemical synthesis and characterization of pure nanometer-sized Fe_3O_4 particles. *Materials Science and Engineering, 286*(1): 101-105.

WHO, World Health Organization. (2004).*Guidelines for drinking-water quality* (3rd ed.). Geneva, Switzerland: WHO.

Wu, W., He, Q. and Jiang, C. (2008). Magnetic iron oxide nanoparticles: synthesis and surface functionalization strategies. *Nanoscale Research Letter, 3*(11): 397-415.

Xin, X. (2012). Highly efficient removal of heavy metal ions by amine-functionalized mesoporous Fe_3O_4 nanoparticles. *Chemical Engineering Journal, 184*: 132-140.

Yamaura, M., Camilo, R.L., Sampaio, L.C., Macedo, M.A., Nakamura, M. and Toma, H.E. (2004). Preparation and characterization of (3-aminopropyl) triethoxysilane-coated magnetite nanoparticles. *Journal of Magnetism and Magnetic Materia, 279*(2-3): 210-217.

Yuan, P., Fan, M., Yang, D., He, H., Liu, D., Yuan, A., Zhu, J. and Chen, T. (2009). Montmorillonite-supported magnetite nanoparticles for the removal of hexavalent chromium Cr (VI) from aqueous solutions. *Journal of Hazardous Materials, 166* (2- 3): 821-829.